TU Delft

Delft University of Technology

Hydrothermal carbonization of Typha australis

Influence of stirring rate

Abdeldayem, Omar M.; Al Noman, Md Abdullah; Dupont, Capucine; Ferras, David; Grand Ndiaye, Lat; Kennedy, Maria

DOI
10.1016/j.envres.2023.116777

Publication date
2023

Document Version
Final published version

Published in
Environmental Research

Citation (APA)
Abdeldayem, O. M., Al Noman, M. A., Dupont, C., Ferras, D., Grand Ndiaye, L., & Kennedy, M. (2023). Hydrothermal carbonization of Typha australis: Influence of stirring rate. *Environmental Research*, *236*(2), Article 116777. https://doi.org/10.1016/j.envres.2023.116777

Important note
To cite this publication, please use the final published version (if applicable).
Please check the document version above.

Copyright
Other than for strictly personal use, it is not permitted to download, forward or distribute the text or part of it, without the consent of the author(s) and/or copyright holder(s), unless the work is under an open content license such as Creative Commons.

Takedown policy
Please contact us and provide details if you believe this document breaches copyrights.
We will remove access to the work immediately and investigate your claim.

This work is downloaded from Delft University of Technology.
For technical reasons the number of authors shown on this cover page is limited to a maximum of 10.

Environmental Research 236 (2023) 116777

Contents lists available at ScienceDirect

Environmental Research

journal homepage: www.elsevier.com/locate/envres

Hydrothermal carbonization of *Typha australis*: Influence of stirring rate

Omar M. Abdeldayem [a,b,*], Md Abdullah Al Noman [a], Capucine Dupont [a], David Ferras [a], Lat Grand Ndiaye [c], Maria Kennedy [a,b]

[a] Department of Water Supply, Sanitation, and Environmental Engineering, IHE Delft Institute for Water Education, Westvest 7, 2611AX, Delft, the Netherlands
[b] Department of Water Management, Faculty of Civil Engineering and Geosciences, Delft University of Technology, Stevinweg 1, 2628 CN, Delft, the Netherlands
[c] Department of Physics, University Assane Seck of Ziguinchor, BP.523, Ziguinchor, Senegal

ARTICLE INFO

Keywords:
Hydrochar
Hydrothermal carbonization
Lignocellulosic biomass
Response stirring rate
Surface methodology
Typha australis

ABSTRACT

According to existing literature, there are no conclusive results on the impact of stirring on hydrothermal carbonization (HTC); some studies report a significant impact on the product's properties, while others indicate no influence. This study investigates the influence of stirring rate on several responses and properties of HTC products, including solid mass yield, solid carbon fraction, surface area, surface functional groups, morphology, and the fate of inorganic elements during HTC. Waste biomass was introduced as a feedstock to a 2 L HTC reactor, where the effects of temperature (180–250 °C), residence time (4–12 h), biomass to water (B/W) ratio (1–10%), and stirring rate (0–130 rpm) were investigated. The findings of this study conclusively indicated that the stirring rate does not influence any of the studied responses or properties of hydrochar under the selected experimental conditions used in this study. Nevertheless, the results indicated that a low-stirring rate (5 RPM) is enough to slightly enhanced the heating-up phase of the HTC reactor. For future research, it is recommended to examine the impact of stirring rate on the HTC of other types of biomass using the methodology developed in this study.

Abbreviations

ATR	Attenuated Total Reflection
ANOVA	Analysis of Variance
BET	Brunauer-Emmet-Teller
B/W ratio	Biomass to Water ratio
CCD	Central Composite Design
DOC	Dissolved Organic Carbon
DN	Dissolved Nitrogen
FTIR	Fourier Transform Infrared
HTC	Hydrothermal Carbonization
ICP-OES	Inductively Coupled Plasma Optical Emission Spectroscopy
NREL	National Renewable Energy Laboratory
R^2	Coefficient of Determination
RSM	Response Surface Methodology
SEM	Scanning Electron Microscope

1. Introduction

Hydrothermal carbonization (HTC) is a thermochemical conversion process that operates in the presence of water in the temperature range 180–250 °C, autogenic pressure (2–10 MPa), and residence time that typically varies between one to several hours (Funke and Ziegler, 2010). At HTC operating conditions, water exists in a subcritical phase that allows it to act as a solvent and a catalyst for several reactions, such as hydrolysis, dehydration, decarboxylation, aromatization, and polymerization condensation (Funke and Ziegler, 2010). The target product associated with these conditions is solid hydrochar, possibly used for various applications such as anodes for batteries, solid biofuel, adsorption, or soil-improving material (Sharma et al., 2020).

A liquid product is solubilized from the solid phase during the HTC reaction, composed mainly of organic compounds in addition to inorganic elements, and has been studied by several researchers (Dima et al., 2022; Reza et al., 2013; Smith et al., 2016). Studying the liquid phase has provided valuable insights into our understanding of the pathways of inorganic elements and led to the use of hydrochar for applications such as phosphate recovery and electrochemical storage. The gas phase usually accounts for less than 10% of the used feedstock (dry basis) and

* Corresponding author. Department of Water Supply, Sanitation, and Environmental Engineering, IHE Delft Institute for Water Education, Westvest 7, 2611AX, Delft, the Netherlands.
E-mail addresses: o.m.h.m.abdeldayem@tudelft.nl, o.abdeldayem@un-ihe.org, omar.abdeldayem94@gmail.com (O.M. Abdeldayem).

https://doi.org/10.1016/j.envres.2023.116777
Received 24 May 2023; Received in revised form 25 July 2023; Accepted 27 July 2023
Available online 28 July 2023
0013-9351/© 2023 The Authors. Published by Elsevier Inc. This is an open access article under the CC BY license (http://creativecommons.org/licenses/by/4.0/).

is composed mainly of CO_2 and, to a lesser extent, CH_4 (Volpe and Fiori, 2017).

Some HTC process parameters have been extensively investigated, namely hydrous conditions, temperature, and residence time. Several studies have indicated the importance of a liquid medium in facilitating carbonization. Additionally, water provides an excellent medium for heat transfer avoiding local temperature peaks that might develop due to exothermal reactions (Funke and Ziegler, 2010). Temperature is regarded as the most influential parameter in HTC; when temperature increases, the solid mass yield, in particular, decreases (Nizamuddin et al., 2017). Compared to temperature, residence time has a similar but less pronounced effect on solid mass yield; however, it was shown to increase HTC slurry dewaterability (Ahmed et al., 2021; Ghanim et al., 2016). Several studies indicated that the particle size of lignocellulosic feedstock has less impact on the HTC process compared to temperature and residence time (Lynam et al., 2015; Nizamuddin et al., 2019; Rogalinski et al., 2008).

Several other HTC process conditions, namely heating, cooling, and stirring rates, are usually overlooked in the literature, although they may influence the obtained products. In the case of stirring, Ubene et al. (2022) recently highlighted that it is widely assumed that stirred reactors produce better-quality hydrochar, but without any solid experimental evidence supporting this statement. Indeed, it is rarely mentioned in HTC experiments if stirring was used or not, and when it is the case, which stirring rate and impeller shape was selected.

To our knowledge, only five experimental studies explicitly dealt with stirring rate influence on HTC. Table 1 summarizes the scope of these studies and their contribution related to stirring influence during HTC. The striking fact is the absence of consensus among them. Indeed, three studies reported that the stirring rate influenced HTC (Jung et al., 2021; Sharma and Dubey, 2020; Volpe et al., 2022), while the other two found the stirring rate influence insignificant (Sharma and Dubey, 2020; Sultana et al., 2021).

These discrepant results may be attributed to several reasons. Firstly, most of the studies employed one reactor size for their stirred tests and another for their unstirred tests (Volpe et al., 2022; Jung et al., 2021; Sharma et al., 2020), making comparing results difficult. Secondly, the studies cover different ranges of HTC operating conditions, notably stirring rate, but also temperature, residence time, or biomass to water (B/W) ratio. Additionally, the feedstock used encompasses various materials, from simple sugars – with additives - in powdered form (Jung et al., 2021; Su et al., 2020) to complex lignocellulosic biomass waste of various particle sizes (Sharma and Dubey, 2020; Sultana et al., 2021; Volpe et al., 2022). Lastly, the five studies did not always compare the same outputs. For instance, Volpe et al. (2022) discussed the differences in terms of product yield and organic composition as well as HHV of the hydrochar, while Su et al. (2020) and Jung et al. (2021) focused on the morphological properties of the hydrochar.

The present study systematically investigates the influence of stirring rate in a broad range of temperatures, residence time, and B/W ratio on the HTC of representative lignocellulosic waste biomass, *Typha australis*. For that purpose, the study results include for each experiment (i) the solid and liquid mass yields; (ii) an extensive characterization of the hydrochars obtained, both in terms of compositional and morphological properties; (iii) an extensive characterization of the liquids in terms of composition; and (iv) the temperature profile during the heating-up phase.

2. Methodology

2.1. Feedstock

In this study, *Typha australis,* commonly known as "Typha", was selected as a representative sample of lignocellulosic biomass waste due to its high valorization potential. Indeed, Typha is an invasive species that threaten ecosystems in wetlands and river banks in many locations (Dia et al., 2020), including Western African countries such as Senegal. Typha causes the deterioration of watercourses and changes the food chain via various trophic levels, completely altering ecological systems (Dia et al., 2020). It is estimated that more than 3 million tons of *Typha australis* are in the Senegal River valley alone (Thiam et al., 2017). Mechanical control of Typha is frequently employed, resulting in

Table 1
Summary of previous experimental studies on stirring influence during HTC.

Study	(Volpe et al., 2022)	(Su et al., 2020)	(Jung et al., 2021)	(Sultana et al., 2021)	(Sharma et al., 2019; Su et al., 2020)
Scope of the publication	- Two different reactors sizes were used i.e., 500 mL (stirred) and 50 mL (unstirred) - Temperature (180–250 °C), residence time (1 h), stirring rate (200 rpm), B/W ratio (10%) - Wet biomass was grounded for size reduction - The analysis included • Product yield balance • Proximate analysis • CHONS • HHV, energy densification ratio • TOC	- 2 L reactor was used - Temperature (180–260 °C), residence time (12–24 h), and stirring rate (0–400 rpm) - Mechanical stirrer was used - The study focused on morphological aspects, surface properties, and the yield of the formation of carbon microspheres - Xylose was used as a feedstock - Soft template (F127) was used	- Two different reactors sizes were used i.e., 12 mL (unstirred) and 0.45 L (stirred) - Temperature (200 °C), residence time (1h), stirring rate (100 rpm), and 0.5 M fructose - Anchor stirrer was used - Additives (salts) were added to the feedstock solution - The morphology of the hydrochar particles was studied in detail	- 300 mL reactor was used - Temperature (180–200 °C), residence time (2–4h), stirring rate (400–600 rpm), and B/W ratio (10%) - Feedstock of 1 mm particle size was used	- Two different reactors sizes were used, i.e., 50 mL (unstirred) teflon-lined autoclave reactor and a 750 mL (stirred) stainless steel reactor - Temperature (160–200 °C), residence time (2–24 h), stirring rate (100 rpm). B/W ratio (1:20) and particle size (425–600 μm) - The effect of stirring was investigated with respect to the reaction mechanism, proximate analysis, CHONS, and combustion profiles
Contribution related to stirring	- Stirring in the 500 mL reactor significantly influenced the HTC residues distribution, leading to greater gas production and lower hydrochar mass yields compared to the 50 mL unstirred reactor	- The diameter of the synthesized carbon microspheres decreases by increasing the stirring rate - Sphericity product yield of the carbon microspheres reduces while increasing the stirring rate	- Unstirred experiments resulted in an exhaustive spherical morphology; the stirred samples show a strongly disrupted morphology with very large merged agglomerates	- Stirring rate was one of the factors of the used DOE - The ANOVA indicated the stirring rate insignificance under the conditions tested	- No substantial difference in the coalification extent was observed in the present study compared to the previous study (non-stirred case) - The proximate analysis and combustion profiles were similar for stirred and non-stirred experiments

enormous amounts of unvalorized wet waste, which is either left to rot or burnt openly.

The Typha sample was collected from Dakar Technopole Swamp in Dakar, Senegal. Typha samples were milled several times using a 1 mm knife to have a particle size of approximately 1 mm; then, the resulting samples were dried at 105 °C for 24 h before use. The lignocellulosic sugars and lignin were determined by adapting the standard National Renewable Energy Laboratory (NREL) procedure (Sluiter et al., 2008a). The NREL standard was used to determine the extractives in the biomass (Sluiter et al., 2008c) .

2.2. Design of experiments

An RSM design of experiments accompanied by a full factorial central composite design (CCD) was carried out in this research to get accurate results while minimizing the number of experiments (Álvarez-Murillo et al., 2015; Cheng et al., 2022; Sabio et al., 2016). The studied factors were temperature (180–250 °C), residence time (4–12 h), B/W ratio (1–10%), and stirring rate (0–130 rpm). The range of factors was chosen based on the operational range of HTC in literature (Fernández-Sanromán et al., 2021; Funke and Ziegler, 2010; Lachos-Perez et al., 2022).

The Reynolds number (Re) was employed as a design criterion for the range of stirring rates in the experiment. In stirred vessels, flow is considered laminar when Re < 10 and fully turbulent when Re $> 10^4$ (Cullen, 2009; Sangare et al., 2021). In the HTC vessel, it was assumed that when the flow regime is turbulent, the particles are uniformly distributed, resulting in a homogeneous mixture (Sangare et al., 2021). The Reynolds number presented in Eq. (1) was utilized, revealing that the flow regime was laminar for experimental runs conducted at 0 and 33 rpm. On the other hand, the flow regime was turbulent for the experimental runs conducted at 65, 98, and 130 rpm.

$$Re = \frac{Nd^2\rho}{\mu} \quad (1)$$

Where N (s^{-1}) is the impeller's rotational frequency, d (m) is the diameter of the impeller, ρ ($\frac{kg}{m^3}$) is the density of the mixture, and μ (Pa. s) is the dynamic viscosity of the mixture.

Studying 4 factors led to a total of 30 experiments, which can be found in Table 2. The studied responses were solid mass yield and solid carbon fraction from HTC.

Linear and quadratic regression models were investigated; analysis of variance (ANOVA) was performed for the models and the process parameters to inspect their significance. The regression models were tested using the coefficient of determination R^2 and *p*-value, and the model with the highest R^2 was chosen. The Fischer test (*F*-value) and the *p*-value were used to determine the significance of the developed regression models and the studied process parameters. From the ANOVA, the significance of the independent parameters and their interactions were analyzed. The significance of the model was based on the *p-value* at 95% confidence level; a *p-value* <0.05 indicates the terms' significance (Raheem et al., 2022). The produced regression model equations were used across the studied range of conditions to generate the response surface plots (Antony, 2003). Finally, the model was validated using 2 validation points with conditions illustrated in Table 2. In Table 2, six additional experiments were added to the experimental design for validation and for extending/confirming the findings outside the studied range.

2.3. Reactor setup and procedure

The HTC tests were performed in a 2 L volume high-pressure reactor (Parr series 4530-floor stand reactor). The reactor had a diameter of 10.16 cm and a height of 26.67 cm. The total power of the HTC system was 3450 W, where the heater corresponds to 2000 W of the total power.

Table 2
Total runs of HTC experiments according to central composite design, additional and validation runs.

Run	Temperature (°C)	Residence Time (h)	B/W ratio (%)	Stirring (rpm)
1	215	12	5.5	65
2	198	10	7.75	98
3	198	6	7.75	98
4	215	8	1.0	65
5	250	8	5.5	65
6	233	10	3.25	98
7	215	8	5.5	0
8	215	8	10.0	65
9	215	8	5.5	65
10	215	8	5.5	65
11	233	6	3.25	33
12	198	10	3.25	98
13	198	6	7.75	33
14	198	10	7.75	33
15	215	8	5.5	65
16	198	10	3.25	33
17	215	8	5.5	65
18	215	8	5.5	130
19	233	6	7.75	98
20	215	4	5.5	65
21	180	8	5.5	65
22	233	6	3.25	98
23	215	8	5.5	65
24	233	10	7.75	33
25	233	6	7.75	33
26	198	6	3.25	33
27	233	10	3.25	33
28	233	10	7.75	98
29	198	6	3.25	98
30	215	8	5.5	65
Validation 1	190	5	2.125	21
Validation 2	215	8	3.25	65
Add 01	215	2	5.5	0
Add 02	215	2	5.5	200
Add 03	215	0.5	5.5	0
Add 04	215	0.5	5.5	200

The heating of the reactor was induced by a heating jacket surrounding the reactor. The reactor had two thermocouples, one inside and one between the heater and the reactor. Additionally, the reactor was equipped with a variable-speed motor (½ hp, 230V) for agitation. This study used an anchor shape impeller with a diameter of 9.80 cm and a height of 12.60 cm. The anchor shape impeller was recommended for stirring viscous fluids (Kamla et al., 2020). A schematic of the HTC is available in Fig. S1 in the supplementary material.

For the temperature history, the heating up phase of the reactor was investigated for different stirring rates (0, 5, 17, 65, 130, and 200 rpm) at 215 °C and a 5.5% B/W ratio using the temperature probe inside the HTC reactor.

According to the experimental setup, Typha was loaded into the HTC reactor with the required B/W ratio and a fixed volume of water of 1.3 L. The reactor was then evacuated with grade-6 inert nitrogen gas for 3 min to replace the air in its headspace and create an anoxic environment in the reactor vessel. The reactor was heated to reach the final temperature in 35 min with a heating rate of around 5.5 °C/min. At the end of each run, the stirrer was stopped, and the reactor was allowed to cool down by natural convection. After reaching ambient temperature, 3 gaseous samples (20 mL each) were collected using gas syringes from the HTC outlet valve. The gas meter was then connected to the HTC outlet valve to measure the total volume of released gas during HTC. The reactor was then opened, and its content unloaded. Three 100, 45, and 20 μm sieves were used to filter the liquid hydrochar mixture. The obtained liquid was additionally filtered using a 0.45 μm filtration step. The collected hydrochar was then dried in an oven at 105 °C for 24 h for further characterization. Finally, a liquid sample of 100 mL was collected for further analysis.

2.4. Product mass yield

The solid mass yield is the ratio of the mass of hydrochar to the mass of dried raw biomass, as illustrated in Eq. (2). The ideal gas law was used to estimate the produced mass of CO_2. Then the gas yield was calculated based on the ratio between the mass of gas (assumed to be fully CO_2) to the mass of dried biomass. The liquid yield was calculated based on the difference between the mass of dried biomass and the sum of solid mass yield and gas yield.

$$Solid\ mass\ yield\ (\%) = \frac{Mass\ of\ dried\ hydrochar}{Mass\ of\ dried\ biomass} \times 100 \quad (2)$$

2.5. Gas, liquid, and solid characterization

2.5.1. Gas characterization

The collected gaseous samples from the HTC experiments were analyzed by SCION 456-GC gas chromatograph (GC). Helium (He) gas was used as the carrier gas, while the PORABOND-Q capillary column (25 m in length) was used for separation.

The CarlTech HATKG-12-NR-00752 standard gases (50% CO_2 and CH_4) were used for calibration. A 0.5 mL injection volume was used with a run time of 2 min. The N_2 gas peak was identified at 1.1 min, while the CH_4 and CO_2 peaks were identified at 1.2 min and 1.4 min, respectively.

2.5.2. Liquid characterization

The liquid samples from the HTC were filtered using a 0.45 μm cellulose-acetate membrane filter paper, acidified to a pH below 2, and stored at 4 °C for a maximum of one week prior to being analyzed.

The dissolved organic carbon (DOC) of the liquid sample was analyzed by using a Shimadzu TOCv-cpn analyzer at 720 °C while the dissolved nitrogen (DN) was analyzed by an accompanying module called Shimadzu TN. Avio 200 PerkinElmer Inductively Coupled Plasma Optical Emission Spectroscopy (ICP-OES) was used to analyze inorganics in the liquid phase. All DOC, DN, and ICP OES measurements were performed with triplicate samples to obtain mean values and measure the standard deviations. The uncertainty of the DOC and DN analysis was ±0.5 mg/L, while the uncertainty of the ICP OES ranged between 2 μg and 60 μg depending on the measured element.

2.5.3. Solid characterization

The proximate analysis was carried out for the raw biomass and the hydrochar samples. The volatile matter and moisture content were measured using EN15148-2009 and EN14774–1:2009, respectively. The ash content was determined according to the NREL operating procedure for the determination of ash in biomass (Sluiter et al., 2008b). The fixed carbon was calculated following Eq. (3).

$$Fixed\ Carbon\ (\%) = 100 - Ash\ (dry\ basis\ \%) - Volatile\ matter\ (dry\ basis\ \%) \quad (3)$$

An Elementar Macro cube elemental analyzer was utilized to analyze the raw biomass C, H, N, S content, and hydrochar following the EN15289-2011 standard procedure. This was done by combusting the samples at 1150 °C. The oxygen content was calculated based on the difference. All measurements were performed in duplicates.

The hydrochar samples underwent microwave digestion following the ISO11466 standard procedure to determine the major and minor inorganic elements. The digested samples were then analyzed using Agilent ICP-OES 51110 to determine the major and minor inorganic elements.

Fourier transform infrared (FTIR) analysis was done using a Bruker Alpha FTIR spectrometer equipped with an attenuated total reflection (ATR) crystal to determine the functional groups inside the hydrochar. The spectral range examined was between 4000 and 400 cm^{-1} with a resolution of 4 cm^{-1}.

The Brunauer-Emmet-Teller (BET) technique was used to calculate the specific surface area of hydrochar following the DIN ISO 9277 standard procedure. Samples were dried at 40 °C and milled to a particle size of less than 3.15 mm, and nitrogen was used as the adsorption gas. The degassing was performed under vacuum at a temperature of 150 °C and for a duration of 2 h.

A scanning electron microscope (SEM- JEOL JSM-6010LA) was utilized to inspect the morphology of the raw biomass and hydrochar surfaces. Before investigating the samples, the stubs were double coated with a thin layer of gold (4 and 6 nm) using a JHC-1300 JEOL sputter coater to produce a conductive surface for SEM investigation.

2.6. Carbon and inorganic elements balance

The carbon balance was calculated for all hydrochar samples using Eq. (3). The carbon content in the hydrochar (solid carbon fraction) was measured (in percentage) using an elemental macro cube analyzer. The carbon concentration in the liquid was calculated in mg/L as DOC. For the gas, GC was used to measure the concentration of CO_2 in the gaseous products. The carbon associated with the gas phase was determined by employing the ideal gas law, utilizing the CO_2 concentration (as measured by GC analysis), the total gas volume collected from the HTC vessel outlet at atmospheric pressure, and the temperature recorded at the moment of gas sampling.

$$C_{Raw\ biomass} = C_{hydrochar} + C_{Gas} + C_{liquid} \quad (4)$$

For the calculation of the fate of inorganics, it was assumed that the inorganics would only be found in solid and liquid phases and not get volatilized under HTC conditions.

3. Results and discussions

3.1. Feedstock

The macromolecular composition of the biomass is illustrated in Table 3. The moisture content as received was 89.5% ± 0.5%, which aligns with common wetland plants' moisture content (Zhao et al., 2012).

3.2. Temperature history in the HTC reactor

The temperature history has been investigated inside the reactor during heating up for different stirring rates (0, 5, 17, 65, 130, and 200 rpm) at 215 °C using a 5.5% B/W ratio and 1 mm particle size, as shown in Fig. 1.

At the beginning of the heating-up phase (7–15 min) in Fig. 1, it was observed in the stirred experiments that the temperature at the sampling point varied depending on the stirring rate. The higher the stirring rate, the higher the achieved temperature. From the 15^{th} min onwards, all the stirred experiments yielded the same temperature in the reactor, indicating that a low stirring rate was enough to achieve temperature homogeneity during the heating-up phase. In contrast, the unstirred experiment (0 rpm) showed a significantly different heating-up history,

Table 3
Macromolecular composition and ash concentration of Typha australis on a dry basis.

Macromolecular composition		Percentage (wdb %)
Cellulose		29 ± 3
Hemicellulose	Xylan	10.90 ± 0.04
	Arabinan	1.70 ± 0.03
	Galactan	0.90 ± 0.07
	Mannan	0.5 ± 0.1
	Rhamnan	0.50 ± 0.02
Lignin		23 ± 2
Ash		13.1 ± 0.6
Extractives		19.6 ± 0.6

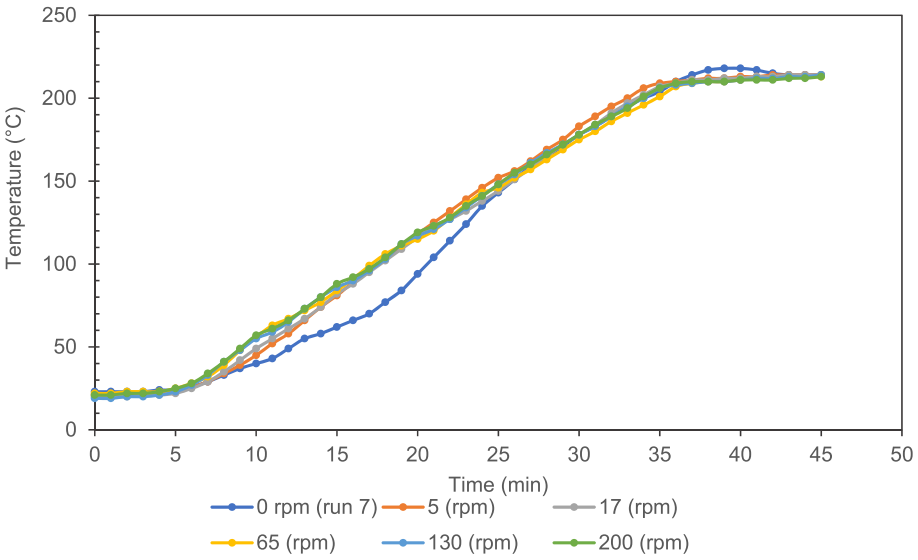


Fig. 1. Temperature history for different stirring rates at 215 °C, and 5.5% B/W ratio.

especially up to the 25th min. The dependency on natural convection for heat transfer probably accounts for the lack of homogeneity in the case of the unstirred experiment. From the 25th min, no significant differences between the heating-up profiles could be noticed. Hence, the stirring rate appears to influence only the first two-thirds of the heating-up process, that is, between 0 and 25 min. It is worth noting that the unstirred reactor's temperature history was overshot for 5 min reaching 218 °C, instead of 215 °C. Such observation may be related to the lack of stirring; Basso et al. (2016) noticed a similar observation in a 50 mL stainless steel unstirred reactor.

There are several reasons behind the observed trends in the HTC temperature histories and the dynamic evolution of stirring rate influence. Firstly, water is a good medium for transferring and storing heat, avoiding local peaks that might arise during HTC (Funke and Ziegler, 2010). Secondly, the heating-up phase had a duration of 35 min, which is a long heating-up period and thus might be sufficient for natural convection to transfer heat homogeneously in such operating conditions. Thirdly, the particle size used might be considered small enough to mix well due to natural convection (Funke and Ziegler, 2010; Sharma and Dubey, 2020). Further tests with shorter heating-up times, higher heating rates, and more extensive temperature monitoring could provide further insights into stirring effects during the heating-up phase.

As a complement, the full temperature history of a central point (Run 23) is illustrated in Fig. S6 in the supplementary material. The cooling down ramp was logically relatively slow as the reactor was left to cool by natural convection at ambient temperature, taking almost 5 h to reach 50 °C. Some reactions might have continued during this phase, influencing the final product distribution. However, as the cooling down time was the same for all experiments, a relative comparison of the experiments and the influence of the different conditions tested remains valid. It may be useful to fasten the cooling ramp in future studies, using, for instance, methods described by Hoekman et al. (2011) and Basso et al. (2016).

3.3. Mass and carbon balance

A product mass balance is presented in Fig. 2a, where the liquid mass yield was calculated based on the difference between the mass of biomass (on a dry basis) and the mass of the hydrochar and gas yields. Additionally, the standard deviation of the solid mass fraction was calculated based on the replicates at the central point. The solid mass fraction was between 30% and 70% based on the process conditions. Liquid composition was between 40% and 70%, depending on the temperature and the amount of biomass. Run 5 demonstrated the lowest solid mass yield, which is attributed to the high severity of the process conditions (250 °C and 8 h) compared to the other runs, in alignment with the literature (Heidari et al., 2019).

The gas composition was between 1% and 7%. The magnitude of gas production depended mainly on the B/W ratio and the temperature used. These results align with Volpe and Fiori (2017) and Stemann et al. (2013).

A carbon balance was also developed for all runs, including the solid, liquid, and gas products, as shown in Fig. 2b. The standard deviation for the carbon mass balance was calculated based on duplicate samples of the carbon fraction in the solid, liquid, and gas phases. The total retrieved carbon content ranged from 87% to 99% relative to the original carbon content in the raw biomass, which aligned with previous studies performed using the same reactor (Arrieta, 2021; Qatarneh et al., 2021). The losses can be explained mainly by hydrochar that adhered to the reactor walls and possible losses during the extraction of the solid, liquid, and gas products.

The majority of carbon in the raw biomass was concentrated in the produced hydrochar (between 47 and 75 db%), while the carbon content in the liquid product varied between 21 and 44% at different operating conditions. The carbon content in the gas product was found to be less than 5%. The carbon balance shows that a higher temperature leads to a higher fraction of carbon in the liquid phase. This occurs as increasing the temperature improves the hydrolysis reaction, which is responsible for releasing organic compounds into the liquid phase (Funke and Ziegler, 2010).

3.4. Effect of process parameters

3.4.1. Solid mass yield

The R^2 and the *p*-value were used to determine the best model for solid mass yield. For linear and quadratic models, the *p*-value was <0.05, indicating their significance (95% confidence level). The R^2 was found to be 0.95 and 0.97 for the linear and quadratic equations. Therefore, the quadratic model was chosen to illustrate the solid mass yield as a function of the independent variables.

The mathematical models for process parameters were developed to fit the solid mass yield, as shown in Eq. (5). This equation is in terms of actual factors, which can be utilized for prediction based on given levels of each factor. A simplified equation using the significant factors is shown in Eq. (6).

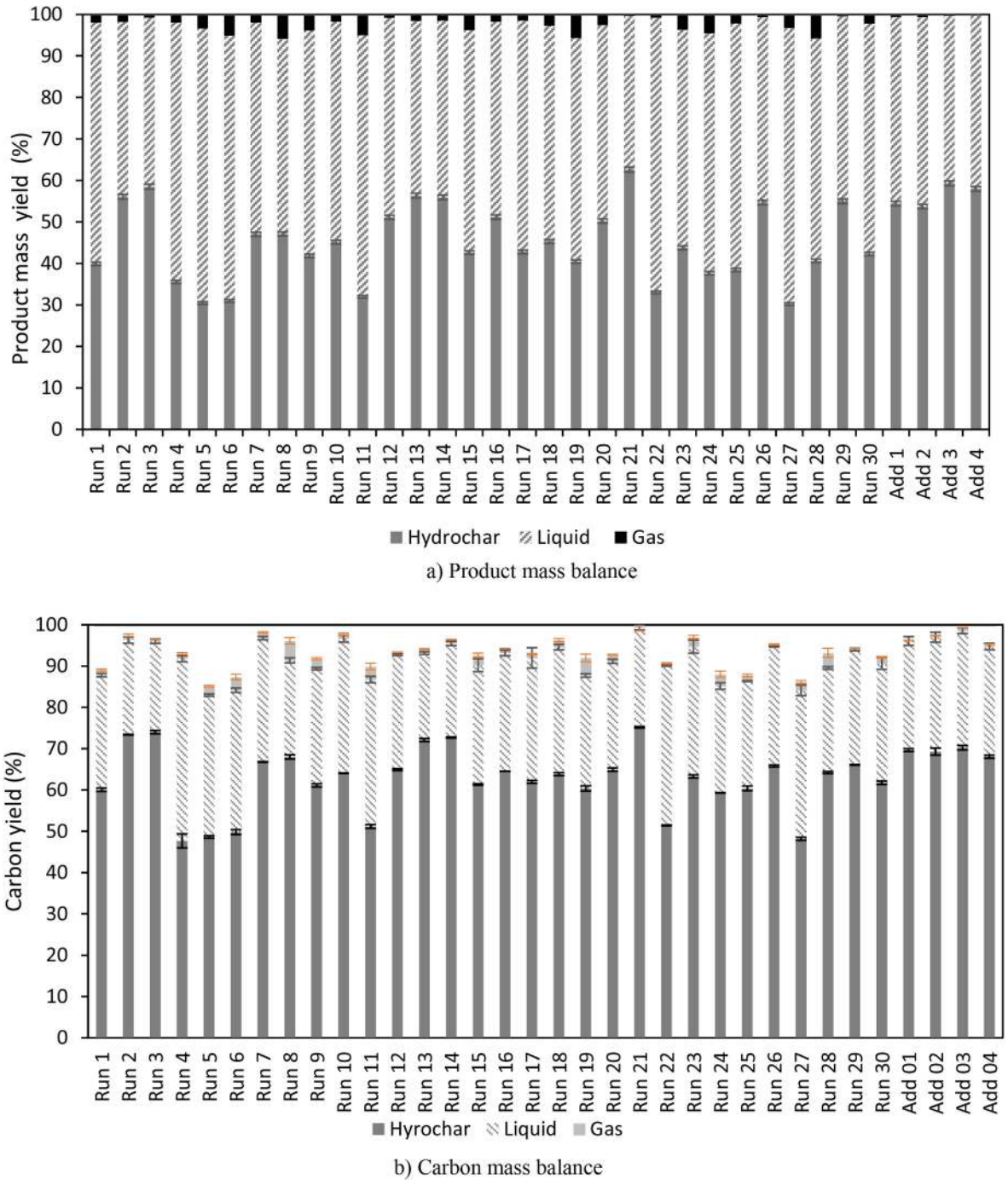


Fig. 2. (a) Product mass balance of all runs, (b) Carbon mass balance of all runs.

$$\textit{Solid mass yield}\ (\%) = 354.96 - 2.11A - 4.29B - 3.24C - 0.074D + 0.0055AB + 0.021AC + 0.00016AD + 0.069BC - 0.0042BD + 0.0021CD + 0.0033A^2 + 0.14B^2 - 0.074C^2 + 0.000552D^2 \quad (5)$$

$$\textit{Solid mass yield}\ (\%) = 295.96 - 1.82A - 0.79B + 1.22C + 0.0030A^2 \quad (6)$$

where A is temperature (^{o}C), B is residence time (h), C is biomass loading (%), and D is stirring rate (rpm).

Two validation points were used to confirm the accuracy of the regression equations. For validation 1, the experimental solid mass yield was 58%, while the predicted results using Eq. (5) and Eq. (6) were 60% and 57%, respectively. For validation 2, the experimental mass yield was 41%, while the predicted results were 40 and 41% using Eq. (5) and Eq. (6), respectively.

The influence of the studied process parameters and their interactions on the solid mass yield is demonstrated in the three-dimensional response surface plots in Fig. 3. Fig. 3a, 3b, and 3c illustrate the interaction between stirring rate and temperature, residence time, and B/W ratio at the central point. Within the investigated range of conditions, the stirring rate had an insignificant effect on the solid mass yield of Typha. Fig. 3a illustrates the combined effect of stirring rate and temperature. This figure shows that between 180 °C and 250 °C, the solid mass yield decreased from 70 to nearly 30%. A 10% reduction of solid yield was observed with increasing residence time (from 4 to 8h), as perceived in Fig. 3b; however, the stirring rate did not influence the solid mass yield at the studied residence time and stirring rate range.

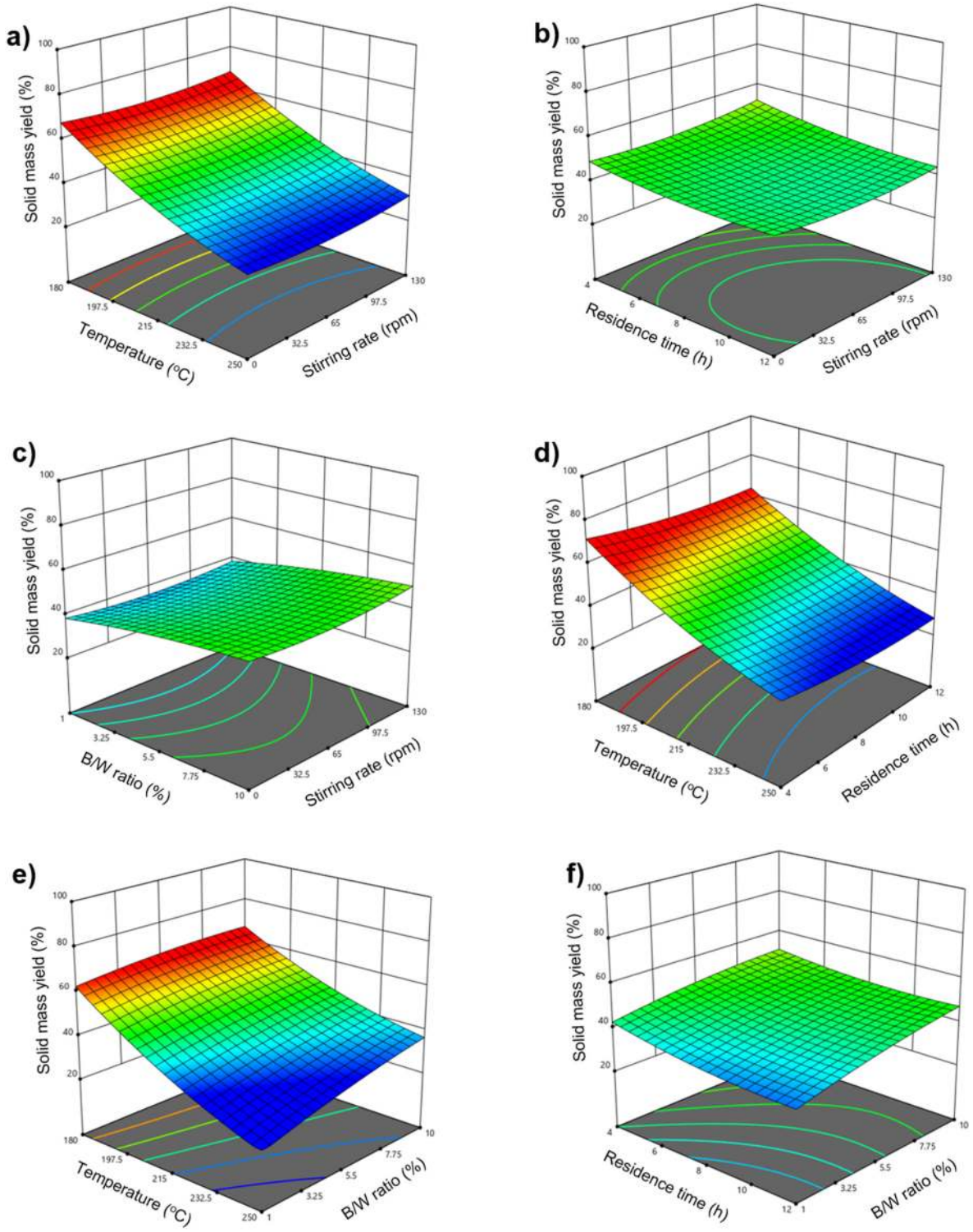


Fig. 3. Influence of different process parameters on the solid mass yield.

Even though it was thought that stirring improves the homogeneity of biomass at higher B/W ratios, no stirring influence on solid mass yield was found in this range of conditions, as shown in Fig. 3c.

The results obtained from the ANOVA confirmed that stirring did not influence the solid mass yield of hydrochar. Moreover, it does not interact with the other process parameters in influencing the solid mass yield within the range of conditions studied here, as the *p*-value of the stirring rate and interactions are >0.05. The factors explaining the absence of influence of stirring rate on the solid mass yield were previously mentioned in section 3.2.

The results obtained from the ANOVA (Table S1 in supplementary materials) indicated that temperature, residence time, and B/W ratio were significant as their *p*-value were <0.05. Fig. 3d illustrates the combined effect of temperature and residence time. The lowest yields were obtained at the highest temperature and residence time (Wang et al., 2018). Additionally, at a lower temperature range of 180 °C, HTC

can degrade hemicelluloses; however, it is ineffective in degrading cellulose or lignin (Koechermann et al., 2018). Hence, at a higher temperature range, significant degradation of cellulose can occur, increasing the formation of secondary hydrochar. Moreover, the increase in the severity of the reaction can strengthen the dehydration and decarboxylation of cellulose and hemicelluloses in the biomass. Specifically, through the aforementioned reactions, a part of the macromolecules underwent direct decomposition and formed gaseous products, such as CO_2, CO, H_2, and CH_4 (Yao and Ma, 2019), while the rest may have undergone hydrolysis and dissolved into the aqueous phase forming intermediates, such as 5-hydroxymethylfurfural, aldehydes, furfural, organic acids (Zhang et al., 2020). Fig. 3e shows that the highest solid mass yield is obtained at lower temperatures and a high B/W ratio. These results were aligned with the findings of Volpe and Fiori (2017). Fig. 3f suggests that the interaction between residence time and B/W ratio only slightly influences the process when the other process parameters are fixed.

Additional experiments were conducted for stirring under more extreme conditions with shorter residence times, as shown by Add 01-Add 04 samples in Table 2 to confirm further the findings related to the stirring rate. For runs Add 01 (0 rpm) and Add 02 (200 rpm), which were conducted at 2 h of residence time, the solid mass yields were 54% for both scenarios. For runs Add 03 (0 rpm) and Add 04 (200 rpm), they were conducted at 30 min residence time and led to a solid mass yield of 58% and 59%, respectively. These results indicated no significant differences. From additional experiments, it can be observed that the relevance of the stirring rate is not influenced by the shorter residence times tested.

3.4.2. Solid carbon fraction

The solid carbon fraction indicates the amount of carbon as a percentage of the final mass of hydrochar. This provides direct insight into properties relevant to energy applications, such as HHV and energy density, or indirect insights for applications, such as soil amendment or electrochemical storage. Overall, the carbon content in the collected hydrochar ranged between 52% and 70%, similar to previous results using similar conditions and feedstock (Chen et al., 2017; Gao et al., 2016).

The R^2 and p-value were used to determine the model that best fits the solid carbon fraction. For all models, the *p*-value was <0.05 indicating their significance. However, the R^2 was found to be 0.92 and 0.91 for the linear and quadratic models. The quadratic model was eliminated as the predicted R^2 and the adjusted R^2 were not close (Adjusted R^2 Predicted $R^2 > 0.2$). Hence, the linear model was chosen to illustrate the solid carbon fraction as a function of the selected independent variables.

The mathematical models for process parameters were developed to fit the hydrochar carbon content, as shown in Eq. (7). A simplified equation using the significant factors is shown in Eq. (8).

$$Solid\ carbon\ fraction(\%) = -17.62 + 0.34A + 0.71B + 0.16C - 0.043D \quad (7)$$

$$Solid\ carbon\ fraction(\%) = -16.99 + 0.34A + 0.71B \quad (8)$$

where A is temperature (^oC), B is residence time (h), C is B/W ratio (%), and D is stirring rate (rpm).

Regarding the validation of the regression equations, two points were used for this purpose. The experimental solid carbon fraction for the first validation experiment was 50%, while the predicted results using Eq. (7) and Eq. (8) gave both 51%. The experimental solid carbon fraction for the second validation experiment was 60%, while the predicted results were 61 and 62% using Eq. (7) and Eq. (8), respectively.

The three-dimensional response surface plots in Fig. 4 illustrate the impact of the studied process parameters on the solid carbon fraction. Fig. 4a, 4b, and 4c demonstrate the interactions of stirring with temperature, residence time, and B/W ratio, respectively.

Similar to the mass yield, it was found that the stirring rate did not significantly influence the carbon content of the hydrochar. Analysis of variance further confirmed these results, i.e., the stirring rate had a *p*-value> 0.05, indicating that it was insignificant for the hydrochar carbon content over the range of operational parameters studied here. The insignificance of the stirring rate on the solid carbon fraction can be attributed to the same reasons as in the case of the solid mass yield illustrated in section 3.4.1.

The ANOVA results demonstrated that the temperature and residence time are the main factors influencing hydrochar carbon content as their *p*-values were <0.05, while the B/W ratio had only a slight influence Fig. 4d shows the combined influence of temperature and residence time. Similar findings were reported by Wilk et al. (2020). Fig. 4e illustrates the combined effects of temperature and B/W ratio. It was observed that the highest hydrochar carbon content was achieved by increasing the temperature. Increasing temperature improves dehydration and decarboxylation reactions (Funke and Ziegler, 2010; Tasca et al., 2020), consequently improving the solid carbon content. The B/W ratio had an insignificant influence on the solid carbon fraction, similar to the findings of Borbolla-Gaxiola et al. (2022). Hence it can be concluded that the temperature had the most significant effect on the solid carbon content, which was confirmed by the ANOVA and is similar to previous studies (Funke and Ziegler, 2010; Tasca et al., 2020). Fig. 4f confirms that residence time and B/W ratio did not significantly impact the carbon content of the hydrochar.

3.4.3. Process water from HTC experiments

Even though the study's primary focus was on the hydrochar properties, the influence of process parameters on the DN and DOC of the process water was also explored. The ANOVA revealed that the *p*-values for the temperature and B/W ratio were <0.05 for DOC and DN under the studied experimental conditions, while the residence time and stirring rate had no significant impact (*p*-value> 0.05) on the DOC and DN during HTC. This might be due to organics and nitrogenous compounds leaching at higher temperatures and B/W ratios.

3.5. Ash content and the fate of inorganics

Ash content has also been investigated (Table S2 in the supplementary materials), and the results indicated that the raw biomass had an ash content was 13.61 db%. In contrast, the experimental runs had an ash content between 4 and 8 db%. It was found that Run05 had the highest ash content; this might be attributed to the high temperature which was employed in this experiment and the possible reincorporation of inorganics in the solid (Smith et al., 2016).

The influence of stirring on the fate of inorganics was studied at three different stirring rates 0, 65, and 130 rpm at HTC conditions of 215 °C, 8h, and 5.5% biomass to water ratio. Fig. 5 shows the distribution of inorganic elements in hydrochar and its liquid products compared to the inorganic elements in raw biomass. The calculated standard deviation was based on triplicate samples obtained for the analysis of the inorganic elements in the solid and liquid phases. Overall, the trends obtained for the three stirring rates were very similar for the majority of the inorganic elements. The alkali and alkaline earth metals such as Ca, Mg, Na, and K leached into the liquid phase due to their higher solubility at low pH, which is similar to the findings of Smith et al. (2016), Arrieta (2021) and Dima et al. (2022). It was reported that organic acids, such as acetic, lactic, formic, and levulinic acid, are produced during HTC through dehydration and decarboxylation reactions (Arrieta, 2021). Hence, this enhances the dissolution of minerals from the feedstock when the process temperature rises during HTC (Kambo and Dutta, 2015).

The highest solid-to-liquid leaching was observed for Na and K, which is similar to the findings of Arrieta (2021). After HTC, other major inorganic elements, such as Al, Fe, and Si, were contained mainly in the hydrochar. Al has a low solubility; therefore, it did not leach

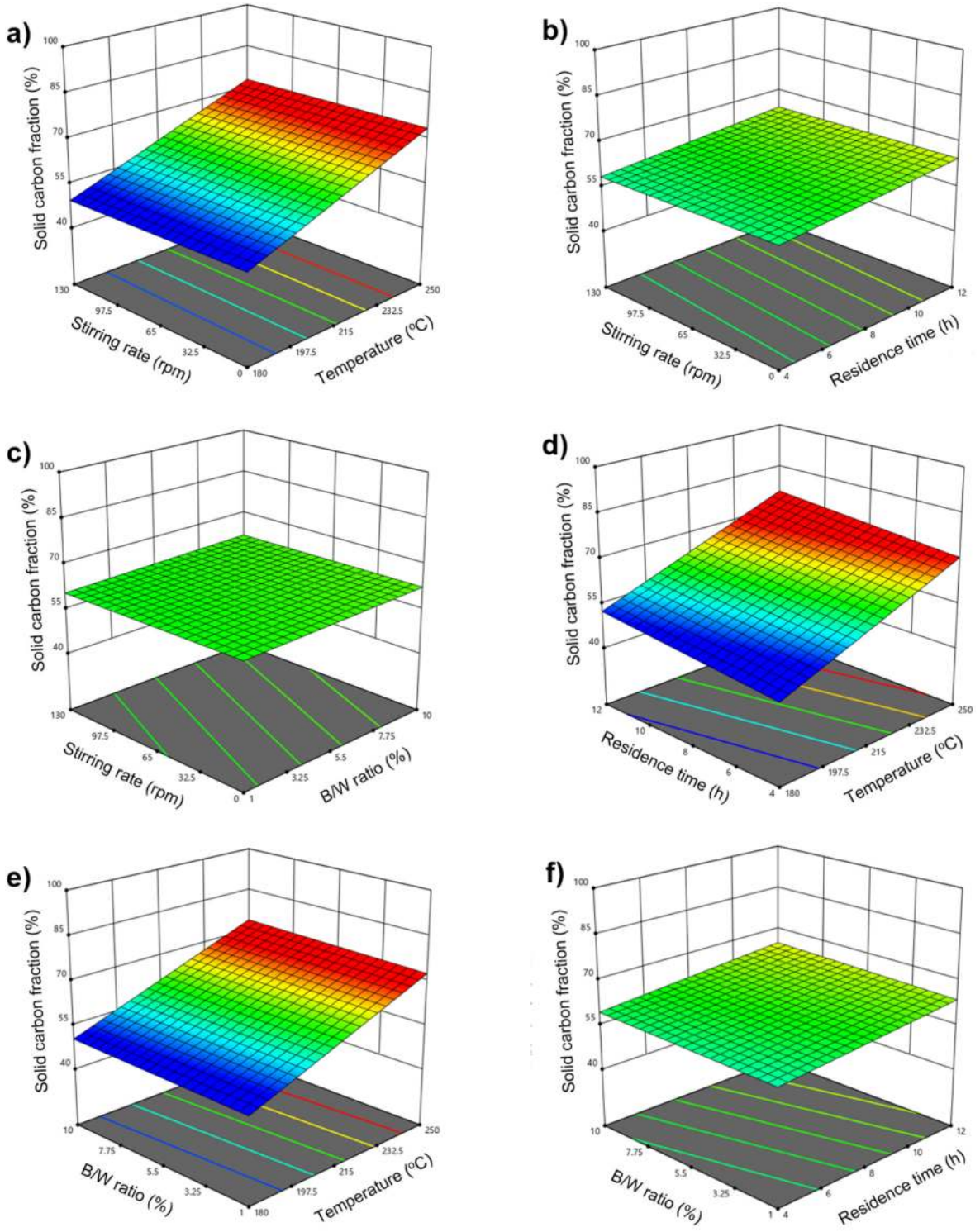


Fig. 4. Influence of different process parameters on the solid carbon fraction.

significantly into the liquid phase. For Fe, an overshoot was seen in the run operated at 0 rpm exceeding the initial inorganic element concentration in raw biomass. This observation is mainly attributed to the reactor's degradation and the possible leaching of Fe from the reactor vessel. This was also reported previously by other researchers working with the same reactor vessel (Arrieta, 2021). Regarding the Si balance, for runs operated at 0 and 130 rpm, most of the Si was contained in the hydrochar, while a small part leached to the liquid phase.

Generally, the error bars are relatively high for minor elements due to their low concentrations. It is worth noting that the majority of Zn was contained in the hydrochar. In contrast with Zn, around 50% of the Mn was contained in the hydrochar, while the rest leached to the liquid phase.

3.6. Dehydration, decarboxylation, and demethanation reactions

The effects of stirring rate and temperature on the H/C and O/C atomic ratios can be visualized in the van Krevelen diagram in Fig. 6, where dehydration, decarboxylation, and demethanation reactions

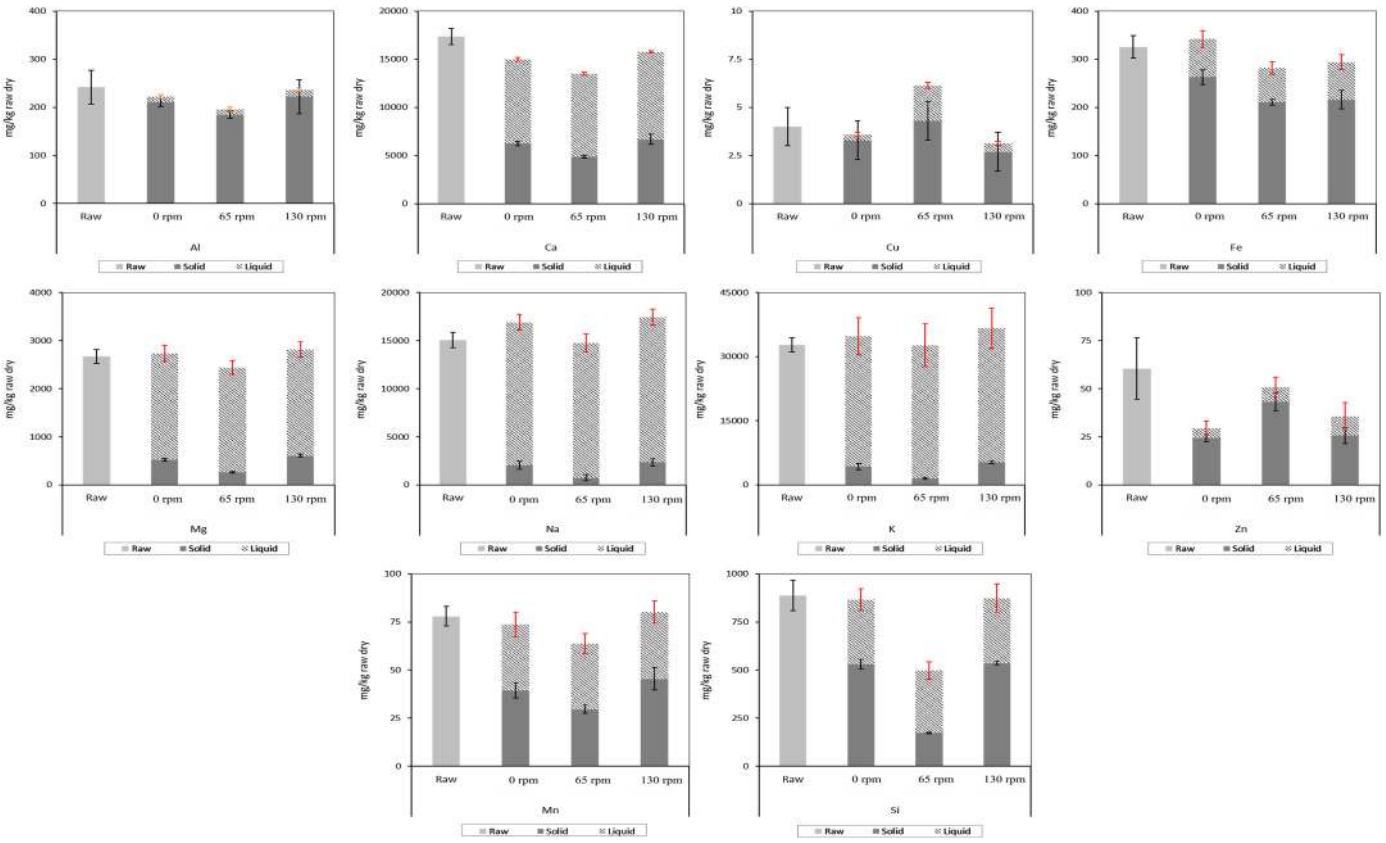


Fig. 5. Fate of inorganics using different stirring rates.

correspond to the arrows. In Fig. 6a, upon increasing the temperature and residence time, the experimental runs shift towards lower H/C and O/C ratios due to dehydration and decarboxylation, as suggested by Fig. 6a (Sharma et al., 2021).

Several duplicate and triplicate experimental results at different stirring rates were plotted in the van Krevelen diagram (Fig. 6b) to investigate the influence of the stirring rate on the studied reactions. The points overlapped well for the runs performed at 0, 65, and 130 rpm, respectively. Similar results were also obtained for other experiments conducted under the same experimental conditions but with different stirring rates. These results indicate that stirring does not seem to influence the reactions under the studied conditions and is aligned with the findings of Sharma and Dubey (2020).

3.7. Hydrochar surface characterization

3.7.1. Surface functional groups

The FTIR spectra for the runs operated at different stirring rates (0, 65, 130 rpm) and 215 °C, 8 h, 5.5% B/W are presented in Fig. S2a (in the supplementary material). In Fig. S2a, it was observed that the graphs show almost no observable differences. Regarding the obtained spectra, the –OH stretching vibration between 3200 and 3400 cm^{-1} demonstrates the presence of phenols and alcohols (Gao et al., 2013). Between 2840 and 2970 cm^{-1}, absorbance peaks correspond to CHn stretching vibrations, a sign for aliphatic and aromatic compounds; gaseous products such as CH_4, C_2H_6, and C_2H_4 are produced when the -C-H functional groups are broken down (Chen et al., 2012). The absorbance peaks obtained between 1800 and 1100 cm^{-1} represents C═O, C═C, and C–O, indicating the release of CO_2; an aromatic ring peak is visualized at 800 cm^{-1} (Gao et al., 2013).

Fig. S2b shows the hydrochar spectra at different temperatures after HTC for 8h, 5.5% B/W ratio, and a stirring rate of 65 rpm. Overall, there are observable differences in the obtained spectra. The intensity of the obtained OH stretching vibration between 3200 and 3400 cm^{-1} was greatest in the case of pristine Typha, while it was the lowest for the hydrochar produced at 250 °C. This suggests that dehydration is more dominant at higher temperatures, leading to a reduction of the –OH stretching vibrations (Gao et al., 2013). Interestingly, the peak obtained between 2840 and 2970 cm^{-1} was similar for the three hydrochars indicating that temperature did not affect the obtained CH_n stretching vibrations. Regarding the absorbance peaks between 1800 and 1200 cm^{-1}, the highest intensity was observed for the hydrochar obtained at 250 °C and the lowest for 180 °C, which confirms the release of more CO_2 at higher temperatures. The peak obtained at 1000 cm^{-1} was the highest for the raw Typha and lowest at the hydrochar produced at 250 °C and is mainly attributed to C–O–H and C–OH functional groups (Niinipuu et al., 2020).

3.7.2. Surface area

The surface area has been analyzed (Table S2 in supplementary materials) for all the produced hydrochar samples. The BET surface area was in the range of 3–10 m^2/g. Such a result appears logical as hydrochars tend to have a low surface area without activation (Adair et al., 2023; Murillo et al., 2022). It was noticed that the studied parameters did not significantly impact the obtained surface area.

3.7.3. Surface morphology

The surface morphology of the raw biomass and the hydrochar was examined using SEM imaging, as illustrated in Fig. S3 (in supplementary material). It can be observed that the raw biomass comprised rigid, smooth, and compact striated fibrils, which can be attributed to the grinding carried out before the analysis. Undergoing HTC on the raw biomass at a temperature of 215 °C led to extra surface degradation, which might be attributed to the total degradation of hemicelluloses and the depolymerization of cellulose, as shown by Zhang et al. (2019). These aspects have increased the amorphous structure in the hydrochar

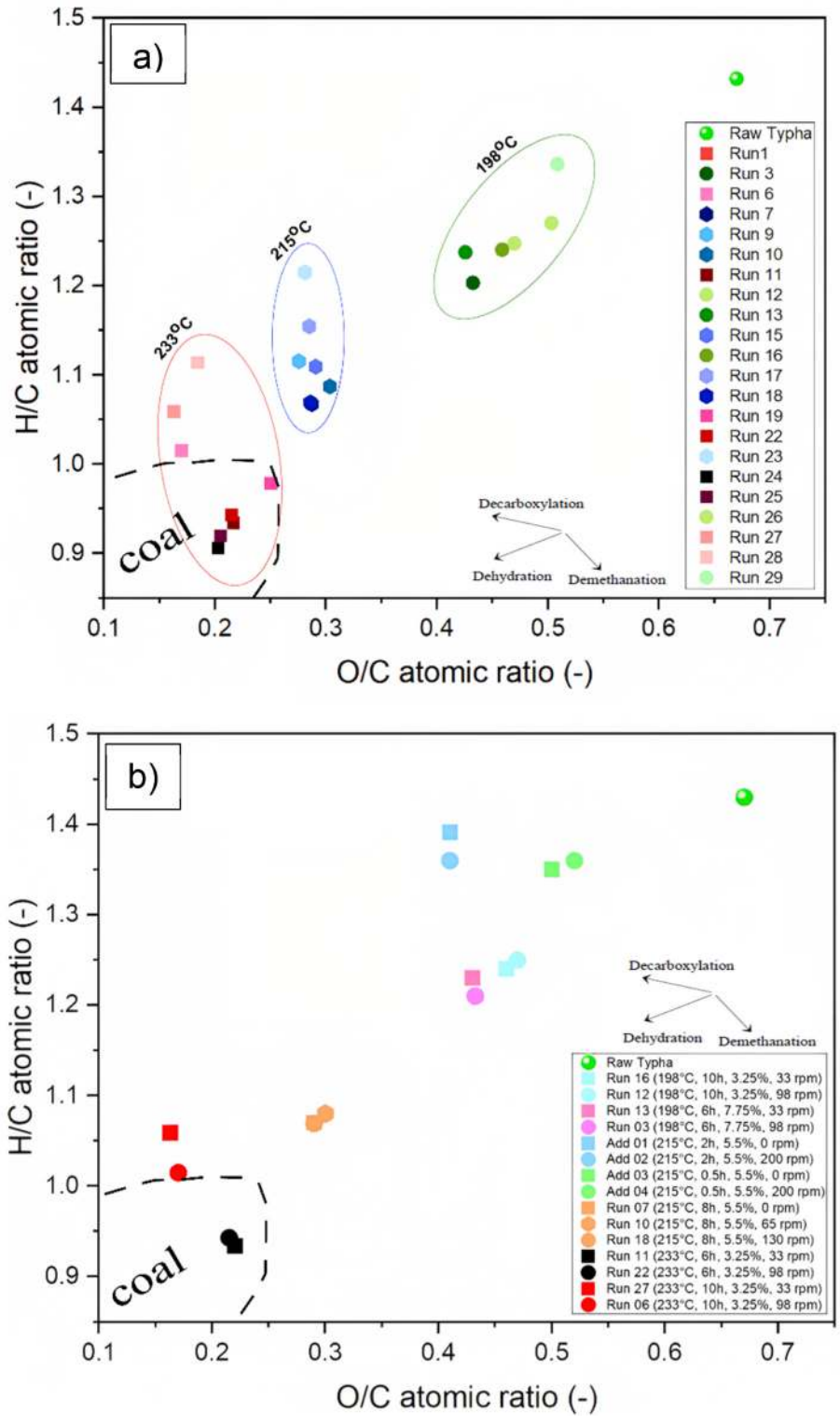


Fig. 6. Van Krevelen diagram based on (a) different temperatures and (b) different stirring rates.

and made the surface rougher than in the raw biomass (Afolabi et al., 2020).

Overall, no observable differences existed between the studied hydrochars from Typha at different stirring rates. This might be attributed to several reasons, such as the biomass's heterogeneity and the insignificance of the stirring rate compared to temperature and residence time under the studied conditions. Unfortunately, no previous studies explored the impact of stirring on hydrochar from lignocellulosic biomass. However, the two previous studies that examined the impact of stirring on pure fructose and D-xylose (Jung et al., 2021; Su et al., 2020) found that stirring had significantly disrupted the morphology of the hydrochar and the microspheres in particular. Such disruption and the microspheres were not observed in the current study, probably due to the fact that complex lignocellulosic biomass was used and not sugars.

4. Practical applications and future prospects

This study can serve as a preliminary guide for applications of Typha-based hydrochar. The produced hydrochar can be used as a soil additive as it contains beneficial elements for plants (Islam et al., 2021). Hydrochar can also be used for carbon sequestration as an additive in construction material or for soil amendment (Masoumi et al., 2021). Furthermore, the hydrochar produced here has a low surface area and can be potentially used as an anode for sodium-ion batteries (Qatarneh et al., 2021). Even though the produced hydrochar has a low surface area, it is rich in functional groups. Hence, it might be used as a low-cost adsorbent, catalyst support, a heterogenous solid acid catalyst, or directly as a catalyst after activation (Masoumi et al., 2021).

For future perspectives, some gaps still need to be addressed to completely understand the effect of stirring. Firstly, the stirring rate needs to be investigated on different types of biomass using the original moisture content and when it is dried, especially at short residence time, e.g., 30 min. Secondly, the usage of different types of impellers is recommended to be studied. Thirdly, the detailed chemistry of the HTC and the exact reaction pathways are still largely unknown (Ischia et al., 2022). Hence, in-depth studies should be carried out to understand HTC chemistry and the influence of stirring rate on it.

5. Conclusions

This study investigated the effects of stirring rate, temperature, residence time, and B/W ratio on several hydrochar properties produced from lignocellulosic waste biomass under the typical HTC range of operations. The findings indicated that the stirring rate did not influence the studied responses and hydrochar properties under selected conditions. Temperature was the most significant parameter, followed by residence time and B/W ratio. Further investigation is recommended using the methodology developed in this study to understand if the conclusions on the stirring rate reported here can be extended to other types of wet biomass.

CRediT authorship contribution statement

Omar Abdeldayem: Methodology, Validation, Formal analysis, Investigation, Data curation, Writing – original draft, Writing – review & editing, Visualization.- **Md Abdullah Al Noman:** Methodology, Investigation, Data curation, Validation- Capucine Dupont: Conceptualization, Methodology, Validation, Resources, Writing – review & editing, Resources, Project administration, Funding acquisition, Supervision.- **David Ferras:** Conceptualization, Methodology, Validation, Resources, Writing – review & editing, Supervision.- **Lat Grand Ndiaye:** Resources, Writing – review & editing.- **Maria Kennedy:** Conceptualization, Methodology, Resources, Writing – review & editing, Supervision.

Funding source

This research has been funded by the Research and Innovation Action project BIO4AFRICA implemented under European Union HORIZON 2020 (Grant Agreement No 101000762).

Declaration of competing interest

The authors declare that they have no known competing financial interests or personal relationships that could have appeared to influence the work reported in this paper.

Data availability

Data will be made available on request.

Acknowledgments

This research has been funded by the Research and Innovation Action project BIO4AFRICA implemented under European Union Funding for Research & Innovation, EU HORIZON 2020 (Grant Agreement No 101000762). The authors thank IHE lab staff: Berend Lolkema and Ferdi Battes. Omar M. Abdeldayem would like to thank Dr. Mostafa Ahmed for his constructive feedback. The authors would like to thank CELIGNIS Ireland for carrying out the required analysis and RAGT Energie for grinding and milling the biomass.

Appendix A. Supplementary data

Supplementary data to this article can be found online at https://doi.org/10.1016/j.envres.2023.116777.

References

Adair, J.L., Karod, M., Goldfarb, J.L., 2023. Addition of in situ clay catalysts at different process points in a cascaded hydrothermal carbonization-pyrolysis process for agro-industrial waste valorization. Bioresour. Technol. 372, 128649.
Afolabi, O.O., Sohail, M., Cheng, Y.L., 2020. Optimisation and characterisation of hydrochar production from spent coffee grounds by hydrothermal carbonisation. Renew. Energy 147, 1380–1391.
Ahmed, M., Andreottola, G., Elagroudy, S., Negm, M.S., Fiori, L., 2021. Coupling hydrothermal carbonization and anaerobic digestion for sewage digestate management: influence of hydrothermal treatment time on dewaterability and bio-methane production. J. Environ. Manag. 281, 111910.
Álvarez-Murillo, A., Román, S., Ledesma, B., Sabio, E., 2015. Study of variables in energy densification of olive stone by hydrothermal carbonization. J. Anal. Appl. Pyrol. 113, 307–314.
Antony, J., 2003. Design of Experiments for Engineers and Scientists. Butterworth-Heinemann, 9780750647090.
Arrieta, M.J.R., 2021. Fate of Biomass Inorganic Elements during Hydrothermal Carbonisation : towards Process Optimisation for Added-Value. IHE Delft for Water Education.
Basso, D., Patuzzi, F., Castello, D., Baratieri, M., Rada, E.C., Weiss-Hortala, E., Fiori, L., 2016. Agro-industrial waste to solid biofuel through hydrothermal carbonization. Waste Manag. 47, 114–121.
Borbolla-Gaxiola, J.E., Ross, A.B., Dupont, V., 2022. Multi-variate and multi-response analysis of hydrothermal carbonization of food waste: hydrochar composition and solid fuel characteristics. Energies 15 (15), 5342.
Chen, Y., Yang, H., Wang, X., Zhang, S., Chen, H., 2012. Biomass-based pyrolytic polygeneration system on cotton stalk pyrolysis: influence of temperature. Bioresour. Technol. 107, 411–418.
Chen, X., Lin, Q., He, R., Zhao, X., Li, G., 2017. Hydrochar production from watermelon peel by hydrothermal carbonization. Bioresour. Technol. 241, 236–243.
Cheng, C., Guo, Q., Ding, L., Raheem, A., He, Q., Lam, S.S., Yu, G., 2022. Upgradation of coconut waste shell to value-added hydrochar via hydrothermal carbonization: parametric optimization using response surface methodology. Appl. Energy 327, 120136.
Cullen, P.J. (Ed.), 2009. Food Mixing: Principles and Applications. John Wiley & Sons.
Dia, B.M., Diagne, M.L., Goudiaby, M.S., 2020. Optimal control of invasive species with economic benefits: application to the Typha proliferation. Nat. Resour. Model. 33 (2), e12268.
Dima, S.S., Arnob, A., Salma, U., Kabir, K.B., Kirtania, K., 2022. Fate of nutrients during hydrothermal carbonization of biogenic municipal waste. Biomass Conver. Biorefinery 12, 71–80.
Fernández-Sanromán, Á., Lama, G., Pazos, M., Rosales, E., Sanromán, M.Á., 2021. Bridging the gap to hydrochar production and its application into frameworks of bioenergy, environmental and biocatalysis areas. Bioresour. Technol. 320, 124399.
Funke, A., Ziegler, F., 2010. Hydrothermal carbonization of biomass: a summary and discussion of chemical mechanisms for process engineering. Biofuels, Bioprod. Biorefining 4 (2), 160–177.
Gao, Y., Wang, X., Wang, J., Li, X., Cheng, J., Yang, H., Chen, H., 2013. Effect of residence time on chemical and structural properties of hydrochar obtained by hydrothermal carbonization of water hyacinth. Energy 58, 376–383.
Gao, P., Zhou, Y., Meng, F., Zhang, Y., Liu, Z., Zhang, W., Xue, G., 2016. Preparation and characterization of hydrochar from waste eucalyptus bark by hydrothermal carbonization. Energy 97, 238–245.
Ghanim, B.M., Pandey, D.S., Kwapinski, W., Leahy, J.J., 2016. Hydrothermal carbonisation of poultry litter: effects of treatment temperature and residence time on yields and chemical properties of hydrochars. Bioresour. Technol. 216, 373–380.
Heidari, M., Norouzi, O., Salaudeen, S., Acharya, B., Dutta, A., 2019. Prediction of hydrothermal carbonization with respect to the biomass components and severity factor. Energy Fuel. 33 (10), 9916–9924.
Hoekman, S.K., Broch, A., Robbins, C., 2011. Hydrothermal carbonization (HTC) of lignocellulosic biomass. Energy Fuel. 25 (4), 1802–1810.
Ischia, G., Cutillo, M., Guella, G., Bazzanella, N., Cazzanelli, M., Orlandi, M., Miotello, A., Fiori, L., 2022. Hydrothermal carbonization of glucose: Secondary char properties, reaction pathways, and kinetics. Chem. Eng. J. 449, 137827.

Islam, M.A., Limon, M.S.H., Romić, M., Islam, M.A., 2021. Hydrochar-based soil amendments for agriculture: a review of recent progress. Arabian J. Geosci. 14, 1–16.
Jung, D., Duman, G., Zimmermann, M., Kruse, A., Yanik, J., 2021. Hydrothermal carbonization of fructose—effect of salts and reactor stirring on the growth and formation of carbon spheres. Biomass Conver. Biorefinery 1–17.
Kambo, H.S., Dutta, A., 2015. A comparative review of biochar and hydrochar in terms of production, physico-chemical properties and applications. Renew. Sustain. Energy Rev. 45, 359–378.
Kamla, Y., Ameur, H., Karas, A., Arab, M.I., 2020. Performance of new designed anchor impellers in stirred tanks. Chem. Pap. 74 (3), 779–785.
Koechermann, J., Goersch, K., Wirth, B., Mühlenberg, J., Klemm, M., 2018. Hydrothermal carbonization: temperature influence on hydrochar and aqueous phase composition during process water recirculation. J. Environ. Chem. Eng. 6 (4), 5481–5487.
Lachos-Perez, D., Torres-Mayanga, P.C., Abaide, E.R., Zabot, G.L., De Castilhos, F., 2022. Hydrothermal carbonization and Liquefaction: differences, progress, challenges, and opportunities. Bioresour. Technol. 343, 126084.
Lynam, J.G., Reza, M.T., Yan, W., Vásquez, V.R., Coronella, C.J., 2015. Hydrothermal carbonization of various lignocellulosic biomass. Biomass Conver.and Biorefinery 5, 173–181.
Masoumi, S., Borugadda, V.B., Nanda, S., Dalai, A.K., 2021. Hydrochar: a review on its production technologies and applications. Catalysts 11 (8), 939.
Murillo, H.A., Pagés-Díaz, J., Díaz-Robles, L.A., Vallejo, F., Huiliñir, C., 2022. Valorization of oat husk by hydrothermal carbonization: optimization of process parameters and anaerobic digestion of spent liquors. Bioresour. Technol. 343, 126112.
Niinipuu, M., Latham, K.G., Boily, J.F., Bergknut, M., Jansson, S., 2020. The impact of hydrothermal carbonization on the surface functionalities of wet waste materials for water treatment applications. Environ. Sci. Pollut. Control Ser. 27, 24369–24379.
Nizamuddin, S., Baloch, H.A., Griffin, G.J., Mubarak, N.M., Bhutto, A.W., Abro, R., et al., 2017. An overview of effect of process parameters on hydrothermal carbonization of biomass. Renew. Sustain. Energy Rev. 73, 1289–1299.
Nizamuddin, S., Qureshi, S.S., Baloch, H.A., Siddiqui, M.T.H., Takkalkar, P., Mubarak, N. M., et al., 2019. Microwave hydrothermal carbonization of rice straw: optimization of process parameters and upgrading of chemical, fuel, structural and thermal properties. Materials 12 (3), 403.
Qatarneh, A.F., Dupont, C., Michel, J., Simonin, L., Beda, A., Ghimbeu, C.M., et al., 2021. River driftwood pretreated via hydrothermal carbonization as a sustainable source of hard carbon for Na-ion battery anodes. J. Environ. Chem. Eng. 9 (6), 106604.
Raheem, A., Ding, L., He, Q., Mangi, F.H., Khand, Z.H., Sajid, M., et al., 2022. Effective pretreatment of corn straw biomass using hydrothermal carbonization for co-gasification with coal: response surface Methodology–Box Behnken design. Fuel 324, 124544.
Reza, M.T., Lynam, J.G., Uddin, M.H., Coronella, C.J., 2013. Hydrothermal carbonization: fate of inorganics. Biomass Bioenergy 49, 86–94.
Rogalinski, T., Ingram, T., Brunner, G., 2008. Hydrolysis of lignocellulosic biomass in water under elevated temperatures and pressures. J. Supercrit. Fluids 47 (1), 54–63.
Sabio, E., Álvarez-Murillo, A., Román, S., Ledesma, B., 2016. Conversion of tomato-peel waste into solid fuel by hydrothermal carbonization: influence of the processing variables. Waste Manag. 47, 122–132.
Sangare, D., Bostyn, S., Moscosa-Santillan, M., Gökalp, I., 2021. Hydrodynamics, heat transfer and kinetics reaction of CFD modeling of a batch stirred reactor under hydrothermal carbonization conditions. Energy 219, 119635.
Sharma, H.B., Dubey, B.K., 2020. Binderless fuel pellets from hydrothermal carbonization of municipal yard waste: effect of severity factor on the hydrochar pellets properties. J. Clean. Prod. 277, 124295.
Sharma, R., Jasrotia, K., Singh, N., Ghosh, P., Srivastava, S., Sharma, N.R., et al., 2020. A comprehensive review on hydrothermal carbonization of biomass and its applications. Chem. Africa 3, 1–19.
Sharma, H.B., Panigrahi, S., Dubey, B.K., 2019. Hydrothermal carbonization of yard waste for solid bio-fuel production: Study on combustion kinetic, energy properties, grindability and flowability of hydrochar. Waste Management 91, 108–119.
Sharma, H.B., Panigrahi, S., Dubey, B.K., 2021. Food waste hydrothermal carbonization: study on the effects of reaction severities, pelletization and framework development using approaches of the circular economy. Bioresour. Technol. 333, 125187.
Sluiter, A., Hames, B., Ruiz, R., Scarlata, C., Sluiter, J., Templeton, D., Crocker, D.L.A.P., 2008a. Determination of structural carbohydrates and lignin in biomass. Lab. Anal. Proced. 1617 (1), 1–16.
Sluiter, A., Hames, B., Ruiz, R., Scarlata, C., Sluiter, J., Templeton, D., 2008b. Determination of Ash in Biomass. Laboratory Analytical Procedure (LAP), Golden, CO, USA, pp. 1–9.
Sluiter, A., Ruiz, R., Scarlata, C., Sluiter, J., Templeton, D., 2008c. Determination of extractives in biomass. In: Laboratory Analytical Procedure (LAP). National Renewable Energy Laboratory, Golden, CO, USA, pp. 1–9.
Smith, A.M., Singh, S., Ross, A.B., 2016. Fate of inorganic material during hydrothermal carbonisation of biomass: influence of feedstock on combustion behaviour of hydrochar. Fuel 169, 135–145.
Stemann, J., Putschew, A., Ziegler, F., 2013. Hydrothermal carbonization: process water characterization and effects of water recirculation. Bioresour. Technol. 143, 139–146.
Su, J., Fang, C., Yang, M., Cheng, Y., Wang, Z., Huang, Z., You, C., 2020. A controllable soft-templating approach to synthesize mesoporous carbon microspheres derived from d-xylose via hydrothermal method. J. Mater. Sci. Technol. 38, 183–188.
Sultana, A., Novera, T.M., Islam, M.A., Limon, S.H., Islam, M.A., 2021. Multi-response Optimization for the Production of *Albizia Saman* Bark Hydrochar through Hydrothermal Carbonization: Characterization and Pyrolysis Kinetic Study. Biomass Conversion and Biorefinery, pp. 1–15.
Tasca, A.L., Stefanelli, E., Raspolli Galletti, A.M., Gori, R., Mannarino, G., Vitolo, S., Puccini, M., 2020. Hydrothermal carbonization of sewage sludge: analysis of process severity and solid content. Chem. Eng. Technol. 43 (12), 2382–2392.
Thiam, A., Mbow, C., Faye, M., Stouffs, P., Azilinon, D., 2017. Assessment of hybrid concentrated solar power-biomass plant generation Potential in Sahel: case study of Senegal. Nat. Resour. 8 (8), 531–547.
Ubene, M., Heidari, M., Dutta, A., 2022. Computational modeling approaches of hydrothermal carbonization: a critical review. Energies 15 (6), 2209.
Volpe, M., Fiori, L., 2017. From olive waste to solid biofuel through hydrothermal carbonisation: the role of temperature and solid load on secondary char formation and hydrochar energy properties. J. Anal. Appl. Pyrol. 124, 63–72.
Volpe, M., Picone, A., Luz, F.C., Mosonik, M.C.A., Volpe, R., Messineo, A., 2022. Potential pitfalls on the scalability of laboratory-based research for hydrothermal carbonization. Fuel 315, 123189.
Wang, T., Zhai, Y., Zhu, Y., Li, C., Zeng, G., 2018. A review of the hydrothermal carbonization of biomass waste for hydrochar formation: process conditions, fundamentals, and physicochemical properties. Renew. Sustain. Energy Rev. 90, 223–247.
Wilk, M., Magdziarz, A., Kalemba-Rec, I., Szymańska-Chargot, M., 2020. Upgrading of green waste into carbon-rich solid biofuel by hydrothermal carbonization: the effect of process parameters on hydrochar derived from acacia. Energy 202, 117717.
Yao, Z., Ma, X., 2019. Hydrothermal carbonization of Chinese fan palm. Bioresour. Technol. 282, 28–36.
Zhang, X., Li, Y., Wang, M., Han, L., Liu, X., 2019. Effects of hydrothermal carbonization conditions on the combustion and kinetics of wheat straw hydrochar pellets and efficiency improvement analyses. Energy Fuel. 34 (1), 587–598.
Zhang, C., Ma, X., Huang, T., Zhou, Y., Tian, Y., 2020. Co-hydrothermal carbonization of water hyacinth and polyvinyl chloride: optimization of process parameters and characterization of hydrochar. Bioresour. Technol. 314, 123676.
Zhao, F., Xi, S., Yang, X., Yang, W., Li, J., Gu, B., He, Z., 2012. Purifying eutrophic river waters with integrated floating island systems. Ecol. Eng. 40, 53–60.